PERGAMON

Micron 34 (2003) 141–155

micron

www.elsevier.com/locate/micron

Thermal diffuse scattering in sub-angstrom quantitative electron microscopy—phenomenon, effects and approaches

Zhong Lin Wang*

School of Materials Science and Engineering, Georgia Institute of Technology, Atlanta, GA 30332-0245, USA

Dedicated to Professor Elmar Zeitler on the occasion of his 75th birthday.

Abstract

This paper reviews the recent progress in the following areas. (1) In quantitative high-resolution transmission electron microscopy, the theoretically calculated images usually give better contrast than the experimentally observed ones although all of the factors have been accounted for. This discrepancy is suggested due to thermal diffusely scattered (TDS) electrons, which were not included in the image calculation. The contribution from TDS electrons is especially important if the image resolution is approaching 0.1 nm and beyond with the introduction of Cs corrected microscopes. A more rigorous multislice theory has been developed to account for this effect. (2) We proved that the off-axis holography is an ideal energy filter that even filters away the contribution made by TDS electrons in the electron wave function, but conventional high-resolution microscopy do contain the contribution made by phonon scattered electrons. (3) In electron scattering, most of the existing dynamical theories have been developed under the first order diffuse scattering approximation, thus, they are restricted to cases where the lattice distortion is small. A formal dynamical theory is presented for calculating diffuse scattering with the inclusion of multiple diffuse scattering. By inclusion of a complex potential in dynamical calculation, a rigorous proof is given to show that the high order diffuse scattering are fully recovered in the calculations using the equation derived under the distorted wave Born approximation, and more importantly, the statistical time and structure averages over the distorted crystal lattices are evaluated analytically prior numerical calculation. This conclusion establishes the basis for expanding the applications of the existing theories. (4) The 'frozen lattice' model is a semi-classical approach for calculating electron diffuse scattering in crystals arisen from thermal vibration of crystal atoms. Based on a rigorous quantum mechanical phonon excitation theory, we have proved that the frozen lattice mode is an excellent approximation and no detectable error would be possible under normal experimental conditions.

Keywords: Phonon; Scattering; Absorption potential; Holography

1. Introduction

There are several main advances in the instrumentation of electron microscopy in recent years. First, the development of monochromator narrows the electron energy spread to the order of meV range, which not only drastically reduces the chromatic aberration effect but also allows much improved beam coherence. The implementation of the energy filter gives us the capability of selecting the energy of the output signals for imaging and diffraction. The energy filter filters off the contribution made by inelastically scattered electrons with energy losses larger than a few eV, thus, the calculated results based on elastic scattering theory can be directly compared to the experimental data. The Cs corrector (Batson et al., 2002), the electron holography (Fu et al., 1991) and image reconstruction technique (Zandbergen and Van Dyck, 2000) are powerful approaches not only for extension of the resolution of the electron imaging, but also for retrieving electron phase image. Quantitative electron microscopy with sub-Angstrom image resolution is now experimentally feasible.

With the vast development in experimental approaches, one must re-examine the theories developed before 1960s for image and diffraction calculations to see if any effect that was not important back to then but is vital in today's super-resolution microscopy. We know that an energy filter filters away most of the inelastically scattered electrons, but electrons with an energy-loss less than a sub eV remain in the image formation process. This means that phonon scattered, or thermal diffuse scattered

* Tel.: +1-404-894-8008; fax: +1-404-894-8008.
E-mail address: zhong.wang@mse.gatech.edu (Z.L. Wang).

0968-4328/03/$ - see front matter © 2003 Elsevier Ltd. All rights reserved.
doi:10.1016/S0968-4328(03)00024-6

(TDS), electrons are included in imaging. The theories most popularly used for today's image simulations, however, are for elastic scattering and the contribution made phonon scattering is excluded. This is not a main problem if the image resolution is poorer than 0.2 nm. But as the image resolution is reaching 0.1 nm and even better, an inclusion of phonon scattering in image calculation is mandatory.

The objective of this paper is to illustrate the effect of TDS in sub-Angstrom resolution electron microscopy and electron holography. Some of the recently theoretical approaches developed are reviewed. We first start from the phenomenon of TDS, then address the effects of TDS in several types of image formation process. Finally, we will examine the 'absorption potential' introduced in electron scattering and to show its relationship with high-order TDS.

2. Phonon scattering in electron diffraction

Atomic vibration is the source of phonon scattering. The vibration of each atom consists of many modes having different frequencies and wave vectors. Each mode is known as a phonon. The effect of phonons on electron scattering is characterized by its perturbation on the crystal potential. This perturbation potential may not be periodic, so that diffuse scattering distributed between Bragg beams is generated. Shown in Fig. 1 is an electron diffraction pattern recorded from GaAs, where some diffuse streaks are clearly visible in the vicinity of Bragg spots. These streaks are the result of thermal diffuse scattering due to the excitation of phonons. TDS may have the following characteristics. First, TDS is closely related to the specimen temperature and it increases dramatically as temperature increases. Second, due to the correlation among atom vibrations, fine diffuse scattering streaks are observed, which are usually oriented along the interconnection lines between Bragg spots. Third, the diffuse scattering intensity is distributed at angles other than Bragg angles owing to the non-periodic perturbation to the crystal potential. Finally, the intensity is distributed at higher scattering angles due to large momentum transfer in TDS, but negligible energy-loss. A detailed analysis of the diffuse streaks can give some information about atomic interaction in solids (Wang, 1993). TDS is also mainly responsible to the Kikuchi patterns observed in electron diffraction. A recent dynamic calculation by Omoto et al. (2002) gives excellent agreement with the experimental data.

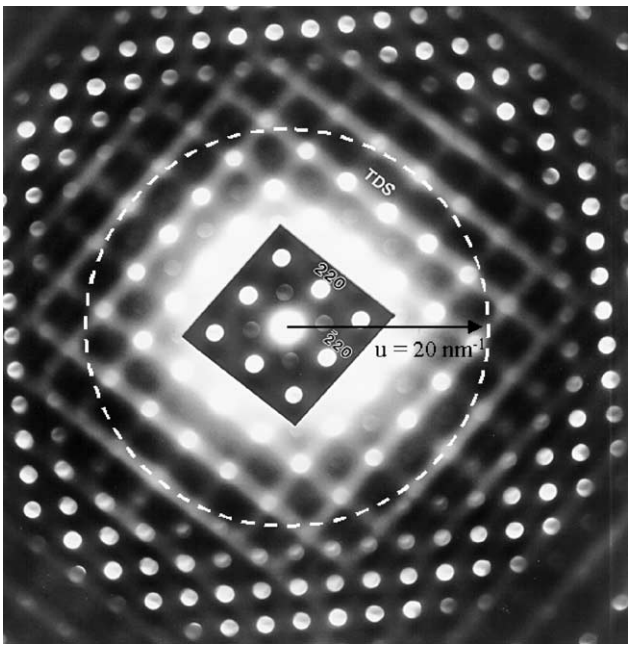

Fig. 1. Electron diffraction pattern recorded from GaAs, showing the presence of diffuse scattering streaks between the Bragg reflections due to thermal vibration of the atoms in the crystals. The circle indicates the frequency corresponding to 0.05 nm resolution. The TDS streaks will strongly affect the contrast of electron image at the atom sites when the image resolution approaches 0.1 nm and beyond.

3. Effects of phonon scattering on elastic wave

Phonon scattering exists in any electron microscopy experiments performed at ambient temperatures. In a general approach, the crystal potential is written as a sum of time-independent and time-dependent components (Takagi, 1958)

$$V(\mathbf{r},t) = V_0(\mathbf{r}) + \Delta V(\mathbf{r},t), \tag{1}$$

where $V_0(\mathbf{r}) = \langle V(\mathbf{r},t)\rangle$ represents the time averaged crystal potential, and it is determined by the equilibrium positions of the atoms and is responsible for the Bragg reflected intensities; and the ΔV term is the perturbation of the thermal vibration on the crystal potential and it is the source of diffuse scattering

$$\Delta V(\mathbf{r},t) = \sum_i [V_i(\mathbf{r} - \mathbf{r}_i - \mathbf{u}_i(t)) - V_{i0}(\mathbf{r} - \mathbf{r}_i)], \tag{2}$$

where $\mathbf{r}_i$ is the equilibrium position of the ith atom (with potential V_i), and $\mathbf{u}_i$ is the time-dependent displacement of the atom from its equilibrium position. $\mathbf{u}_i$ is usually a non-periodic function, and so is ΔV.

To see the relative magnitude of ΔV to V_0, Fig. 2 shows the calculated instantaneous potential V, thermal equilibrium potential V_0, and the difference $\Delta V = V - V_0$ for a silicon atom using the experimentally determined mean square root vibration amplitude of Si. If the instantaneous position of the atom is its equilibrium lattice site, ΔV is a symmetric, sharp function. If the atom is displaced to an instantaneous position located at 0.068 Å on the left-hand side from the equilibrium site, ΔV is no longer symmetric (Fig. 2b). Two striking characteristics are noticed. Firstly, the magnitude of ΔV is comparable with that of V_0 and this

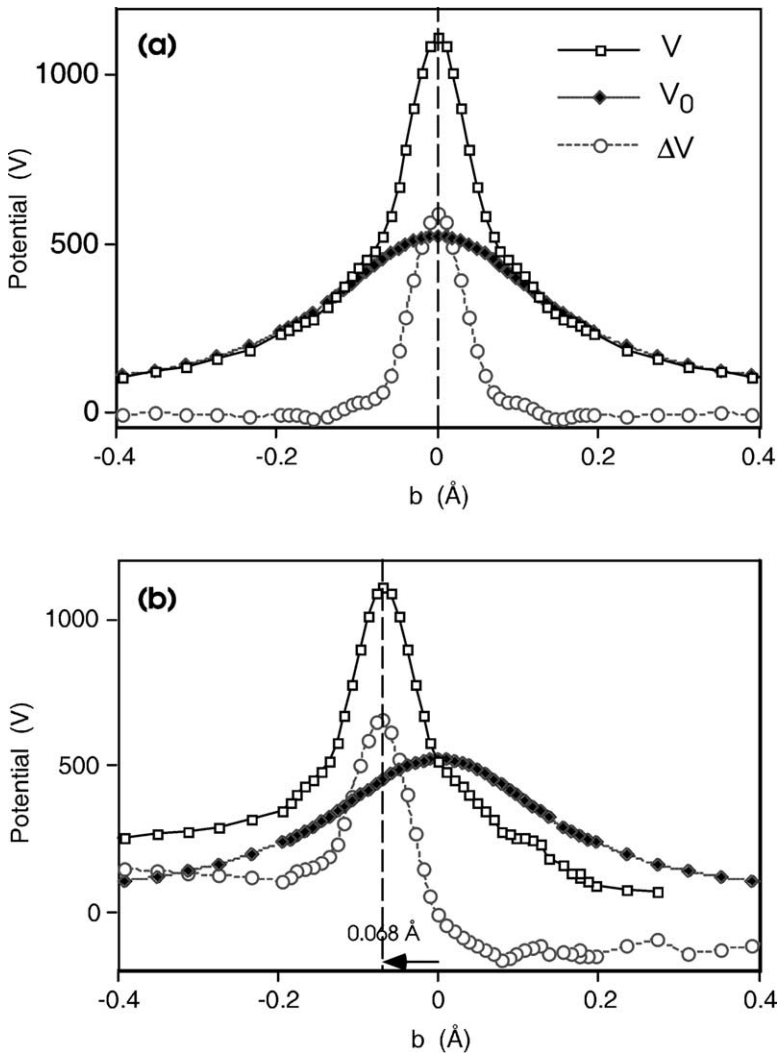

Fig. 2. Potential of a silicon atom with (V_0) and without (V) including the Debye–Waller factor. V is the instantaneous atomic potential and V_0 is the time-averaged atomic potential. The equilibrium position of the atom is $b = 0$. $\Delta V = V - V_0$ (dash-dotted line) is the deviation of the atomic potential from the time averaged potential V_0 when the atomic displacement is (a) $u_\kappa = 0$ or (b) $u_\kappa = -0.068$ Å. The arrowhead in (b) indicates the displacement of the atom. The mean square-root atom vibration amplitude was taken as 0.07 Å in the calculation.

is true for each atom present in the specimen. Secondly, ΔV is considerably narrower than V_0, indicating that TDS is a rather localized scattering process, with the majority of the electrons being generated from the nuclear sites. It is apparent that the TDS is a very localized scattering process. In high-resolution transmission electron microscopy (HRTEM), as the image resolution is approaching 1 Å, the image contrast at the atomic columns is likely to be affected by TDS. It is necessary to take this component into consideration in image calculation if quantitative data analysis is needed.

3.1. The Debye–Waller factor

Vibration of crystal lattices is an important phenomenon in solid state physics, which is a result of thermal motion of crystal atoms. The crystal potential responsible for Bragg reflections is a time averaged potential, which can be conveniently written in its Fourier transform of the electron scattering factor $f_i^e(\tau)$,

$$\begin{aligned} V_0(\mathbf{r}) &= \left\langle \sum_i [V_i(\mathbf{r} - \mathbf{r}_i - \mathbf{u}_i(t)] \right\rangle \\ &= \left\langle \sum_i \int \mathrm{d}\tau f_i^e(\tau) \exp[2\pi i \tau(\mathbf{r} - \mathbf{r}_i - \mathbf{u}_i(t)] \right\rangle \\ &= \sum_i \int \mathrm{d}\tau f_i^e(\tau) \exp[2\pi i \tau(\mathbf{r} - \mathbf{r}_i)] \langle \exp(2\pi i \tau \mathbf{u}_i(t)) \rangle \\ &= \sum_i \int \mathrm{d}\tau f_i^e(\tau) \exp[-W_i(\tau)] \exp[2\pi i \tau(\mathbf{r} - \mathbf{r}_i)], \end{aligned} \quad (3)$$

where $W_i(\tau) = 2\pi^2 \langle |\tau \mathbf{u}_i|^2 \rangle = 2\pi^2 \bar{\mathbf{u}}_i^2 \tau^2$ is the Debye–Waller factor involved in electron diffraction and image calculations, and $\bar{\mathbf{u}}_i^2$ is the mean square displacement of the atom.

This factor depends sensitively on temperature and the structure of the crystal and it is a parameter usually unknown for complex structures, although it has been documented for some simple metals and semiconductors. In the Debye model and under the harmonic oscillator approximation, the Debye–Waller factor can be calculated by Sears and Shelley (1991)

$$\bar{\mathbf{u}}_i^2 = \frac{3\hbar^2}{M_i k_B T_D}\left\{\frac{T^2}{T_D^2}\int_0^{T_D/T} dx \frac{x}{\exp(x)-1} + \frac{1}{4}\right\}, \quad (4)$$

where T_D is the Debye temperature, k_B the Boltzman constant, and M_i the mass of the atom. The Debye–Waller factor has been tabulated using an empirical parameterization approach (Peng et al., 1996).

It is apparent that the Debye–Waller factor is the result of atomic thermal vibration on the periodic potential V_0 of the crystal, which represents the reduction of the Bragg reflected intensities by the atomic vibration. The intensity taken away from the Bragg reflections is distributed between the Bragg angles, e.g. the diffuse scattering. The Debye–Waller factor is a key parameter in quantitative microscopy.

3.2. The absorption potential

In conventional diffraction-contrast imaging, the images are formed by selecting a single Bragg reflected beam using a small objective aperture, so that any electrons inelastically scattered out the angular range of the aperture do not contribute to the image and are thus considered to have been 'absorbed'. From the above discussion, the inelastically scattered electrons will be distributed at angles other than the Bragg angles; thus, they are considered to be effectively absorbed by the crystal as long as the elastically scattered wave is concerned. This is the reason that inelastic scattering is normally considered to be an absorption effect in the imaging of Bragg reflected electrons. The absorption potential is another key quantity in structure determination.

The inclusion of an imaginary potential in the dynamic calculation accounts only for the reduction of the elastic intensity by the inelastic scattering (Yoshioka, 1957). It has not considered the contribution made by the inelastically scattered electrons to the image/diffraction pattern. Inelastically scattered electrons falling inside the angular selection range of the objective aperture do contribute to the image/diffraction pattern. The absorption effect used in electron diffraction is only a phenomenological treatment of the 'loss' of electrons due to inelastic scattering. In practice, the inelastically scattered electrons are not lost but distributed at angles other than the Bragg angles. This is a point that can be easily misunderstood.

The calculation of absorption potential is rather complex, depending on the physical model and the inelastic scattering processes (for a review see Chapter 6 in Wang (1995) and Fanidis et al. (1992, 1993)). The relationship between the absorption potential and multiple diffuse scattering and its calculations will be given in follows.

4. Application of phonon scattered electrons in high-angle annular dark-field STEM imaging

Determining the lattice structure and the atom types filling the lattices are two critical steps in characterization of functional materials. Most of the chemical imaging has been performed in scanning electron microscopy (SEM) and scanning transmission electron microscopy (STEM). The characteristic inelastic scattering signals emitted from the interaction volume of the electron probe with the specimen are determined by the thickness-projected elemental concentrations, provided there is no beam broadening and no fluctuation in incident beam current. X-rays and Auger electrons are acquired sequentially as a function of the electron scanning position. Chemical images obtained using x-ray signals can be directly correlated with the thickness-projected elemental maps in the specimen. The images are more sensitive to elements with large atomic numbers than those with small Z's. The images formed using Auger signals are sensitive to light elements distributed within 1–2 nm into the surface of the specimen.

The dominant contribution of TDS to the annular dark-field STEM image was first proposed by Wang and Cowley (1989, 1990). The localization of phonon excitation can be seen in the calculated single atom scattering factor for elastic and thermal diffuse scattering (Fig. 3). It is apparent that the low angle scattering is dominated by elastic scattering, while the high angle scattering is dominated by TDS. This dominant effect is apparent when the scattering angle is larger than that for the (880) reflection from Si. At the first order Laue zone (FOLZ) position, TDS is about six times stronger than the elastic scattering. In STEM, if an annular-dark-field (ADF) detector is positioned to collect the electrons that are scattered to high angles, the image contrast is insensitive to diffraction and phase contrast but is sensitive to the projected atomic number, because at high scattering angles, the atomic scattering factor is approximated by

$$f_\kappa^e(\mathbf{s}) = \frac{e}{16\pi^2\varepsilon_0}\frac{[Z - f_\kappa^x(\mathbf{s})]}{s^2} \approx \frac{e}{16\pi^2\varepsilon_0}\frac{Z}{s^2} \text{ for large } s, \quad (5)$$

where f^x is the X-ray scattering factor. The scaling of $f_\kappa^e(\mathbf{s})$ with Z is the basis of Z-contrast imaging (Crewe, 1978; Pennycook and Jesson, 1990), provided there is no complication from dynamic electron diffraction effect.

Based on the reciprocity theorem, an analogous Z-contrast image can be formed in TEM using an on-axis objective aperture with hollow cone beam illumination, in which the incident beam strikes the specimen at an angle

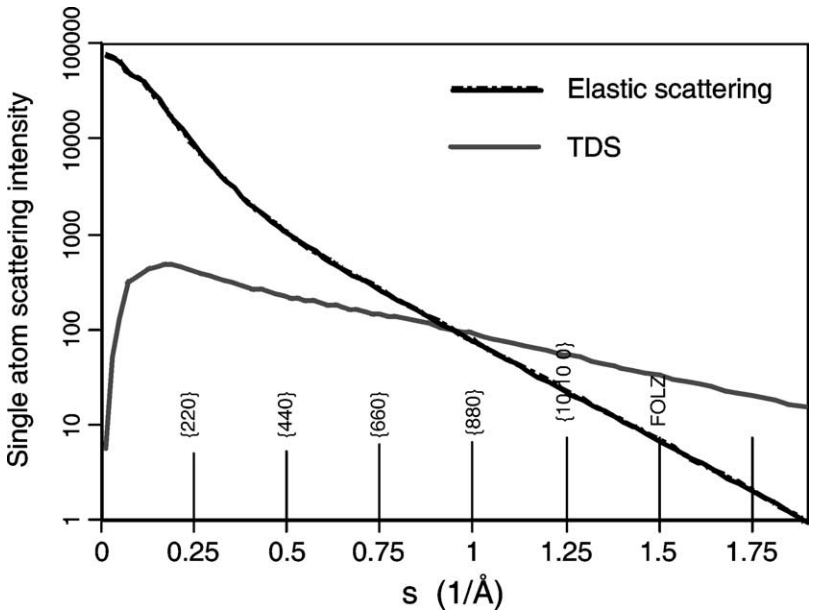

Fig. 3. Theoretically calculated atom scattering factors for elastic scattering $[(f^e)^2\{\exp(-2W)\}]$ and thermal diffuse scattering $[(f^e)^2\{1-\exp(-2W)\}]$ of a Si atom, showing the dominant contribution of TDS at high scattering angles, where W is the Debye–Waller factor. The scattering vector $s = g/2$. The mean square root atomic vibration amplitude was taken as 0.07 Å in the calculation.

and the beam is conically scanned around a circle. Atomic-resolution, Z-dependent images have been achieved (Wang, 1994; Geipel and Mader, 1996; Sidorov et al., 1997). This type of images has characteristics similar to the high-angle ADF-STEM images.

Back scattering is a typical phenomenon of large-angle TDS. Electrons are scattered for an angle larger than 90° without a huge energy-loss. This type of scattering is very sensitive to the atomic number of the scattering source and it has been applied to form the electron backscattered pattern (EBSP) in SEM (Garmestani et al., 1998; Goyal et al., 1997). For a semi-infinite specimen in SEM, the backscattered electrons generated inside the specimen suffer dynamic diffraction by the crystal lattices. The large angle divergence of the TDS results in the formation of Kikuchi pattern, which is a unique representation of the specimen orientation. By indexing the Kikuchi pattern for each of the incident electron probe position, an orientational image can be obtained across the specimen. This is a very useful technique for quantifying the texturing and grain orientational distribution in thin films and bulk specimens.

Backscattered electrons in STEM (or SEM) (Goldstein et al., 1992) give a composition-sensitive image because the atomic backscattering factor is proportional to the average atomic number Z at the beam illumination region due to the dominant roles of Rutherford and thermal diffuse scattering at high angles. This type of image can provide useful information about the average mass density at the local region, but it cannot discriminate the contributions made by different elements.

5. The frozen lattice model for phonon scattering—how accurate is it?

In dealing with the effect of TDS in electron diffraction, a frozen lattice model is usually introduced for the convenience of physical approach (Hirsch et al., 1977), which means that, although atom vibration is a time-dependent process, the crystal lattice appears as if in a stationary instantaneous configuration for an incident electron since the interaction time of the electron with the crystal is much shorter than the vibration period of the crystal atom, but the crystal lattice can be in another configuration for the next incoming electron due to the fact that the average distance between two successive incident electrons is ~1 m in TEM. Thus, for each lattice configuration, the scattering of the electron can be considered as a time-independent quasi-elastic scattering process, and the final observed diffraction pattern/image is equivalent to a time average on the intensities calculated for the different lattice configurations.

This model is the basis of many theoretical approaches for treating phonon scattering (or thermal diffuse scattering, TDS) in electron diffraction/imaging, and a quantitative agreement with experimental observation has been achieved (Loane et al., 1991; Muller et al., 1997). There are, however, two major concerns about this model. First, this is a quasi-elastic scattering model in which the electrons diffusely scattered by one lattice configuration are considered coherent although the scattering from different lattice configurations are treated incoherently. This deviates from the fundamental result of quantum mechanics that phonon scattering is an incoherent process, and phonon excitation is a transition process. Secondly, this

model treats a time-dependent atom vibration process as an integration of many individual time-independent processes. Thus, some semi-classical concept is introduced in this quantum excitation process. Thus, the question is whether this model can give an accurate account of the phonon excitation.

Based on rigorous Green's function and density matrix theories, it has been proved (Wang, 1998a) that the calculation based on the frozen lattice model for thermal diffuse scattering in electron diffraction gives an identical result to that obtained from the phonon excitation model if the following two conditions are satisfied: (1) the incoherence between different orders of thermal diffuse scattering is considered in the frozen lattice model calculation; and (2) the specimen thickness and the mean-free-path length for phonon excitation are both much smaller than the distance traveled by the electron within the life-time of the phonon. Conditions (2) is absolutely satisfied by both low and high energy electrons, and satisfying condition (1) is the most critical requirement in the frozen lattice model calculation. More specifically, the diffuse scattering produced by the different orders of diffuse scattering (such as ΔV^2, ΔV^4 and ΔV^6, etc. or multiple diffuse scattering) must be treated as incoherent in the frozen lattice model, and the higher order scattering is the result of multiple incoherent first order scattering events. This incoherence can be precisely accounted for with the introduction of the mixed dynamic form factor $S(\mathbf{Q},\mathbf{Q}')$ (Wang, 1995b), a key quantity for inelastic electron scattering. A new multislice approach has been proposed recently in which the multiple diffuse scattering and the incoherence effects are both accounted for using the $S(\mathbf{Q},\mathbf{Q}')$ function (Wang, 1998b).

The frozen lattice model can also be used to calculate the diffuse diffraction of low energy electron because their effective penetration depth is relatively small (Wang, 1998a). This conclusion confirms the validity, reliability and accuracy of using the frozen lattice model in numerous dynamic theories of phonon excitation in electron diffraction and imaging of thin specimens. This also removes a restriction that the frozen lattice model is valid only for high-energy electrons.

6. How does phonon scattering affect off-axis electron holography?

Electron holography is a rapidly developing field in electron microscopy and it gives many promises to solve some of the unique problems in materials science and physics (Tonomura, 1993; Fu et al., 1991). An important characteristic of holography is the ability to recover both the amplitude and phase components of the complex exit wave of the object. Electron holograms are the results of electron wave interference. Electrons with appreciable energy-loss have lost their coherence with the incident reference wave, thus, they will not contribute to the interference fringes, automatically being filtered. The question is if the TDS electrons will contribute to the electron hologram. We now use the off-axis electron hologram to examine this problem.

The off-axis electron holography is a two-step imaging technique (Fig. 4). The first step is to form a hologram by means of an electrostatic biprism, inserted, for example, between the back focal plane of the objective lens and the intermediate image plane. The specimen is positioned to cover half of the image plane, leaving the other half of the incident wave for the reference wave $\exp(\mathrm{i}2\pi\mathbf{K}\cdot\mathbf{r})$, which is a plane wave with $\mathbf{K}$ as the wave vector of the incident electrons. By applying a positive voltage to the filament of the biprism, the reference and the object waves on the two sides of the biprism are deflected towards each other, to directions $\mathbf{K}_1$ and $\mathbf{K}_2$, respectively, forming an interference pattern in the image plane, i.e. a hologram. If the exit wave of the object after being modified by the aberration effect of the objective lens and the specimen is represented by $[\exp(\mathrm{i}2\pi\mathbf{K}\cdot\mathrm{r})A(x,y)\exp(\mathrm{i}\phi(x,y))]$, where $A(\mathbf{b},t)$ and $\phi(\mathbf{b},t)$ are real functions describing the amplitude and phase, respectively, the measured intensity distribution in the hologram is

$$\begin{aligned} I_{\mathrm{hol}}(\mathbf{b}) =& \langle|\exp(\mathrm{i}2\pi\mathbf{K}_1\cdot\mathbf{r}) + \exp(\mathrm{i}2\pi\mathbf{K}_2\cdot\mathbf{r})A(\mathbf{b},t) \\ & \times \exp[i\phi(\mathbf{b},t)]|^2\rangle = 1 + \langle A^2(\mathbf{b},t)\rangle + 2\langle A(\mathbf{b},t) \\ & \times \cos[\phi(\mathbf{b},t) + 2\pi\Delta\mathbf{K}\cdot\mathbf{r}]\rangle, \end{aligned} \tag{6}$$

where $\Delta\mathbf{K} = \mathbf{K}_1 - \mathbf{K}_2$. $\langle\ \rangle$ is an average over time, which means that the recorded intensity distribution is the result of electron scattering by the specimen with different thermal vibrational configurations of the lattice.

The second step is to reconstruct the hologram in order to get the object wave. Using the computing reconstruction method, a Fourier transform (FT) of the hologram is taken,

$$\begin{aligned} \mathrm{FT}[I_{\mathrm{hol}}(\mathbf{b})] =& \delta(\mathbf{u}) + \mathrm{FT}[\langle A^2(\mathbf{b},t)\rangle] + \mathrm{FT}[\langle A(\mathbf{b},t) \\ & \times \exp(\mathrm{i}\phi(\mathbf{b},t))\rangle) * \delta(\mathbf{u}+\Delta\mathbf{K}) + \mathrm{FT}[\langle A(\mathbf{b},t) \\ & \times \exp(-\mathrm{i}\phi(\mathbf{b},t))\rangle) * \delta(\mathbf{u}-\Delta\mathbf{K}), \end{aligned} \tag{7}$$

where $*$ indicates a convolution calculation, the $\delta(\mathbf{u})$ function is the transmitted (000) beam; $\mathbf{u}$ is a reciprocal space vector; the second term is the autocorrelation term that is located near the center of the diffraction pattern; and the last two terms are centered at $\mathbf{u} = -\Delta\mathbf{K}$ and $\mathbf{u} = \Delta\mathbf{K}$, respectively, and are the so called 'sidebands'. To see the effect of TDS in Eq. (2), the time-dependent and time-independent parts are separated as

$$\begin{aligned} & A(\mathbf{b},t)\exp[\mathrm{i}\phi(\mathbf{b},t)] \\ & \quad = A_0(\mathbf{b})\exp[i\phi_0(\mathbf{b})] + \Delta A(\mathbf{b},t)\exp[\mathrm{i}\phi'(\mathbf{b},t)], \end{aligned} \tag{8a}$$

where

$$A_0(\mathbf{b})\exp[\mathrm{i}\phi_0(\mathbf{b})] = \langle A(\mathbf{b},t)\exp[\mathrm{i}\phi(\mathbf{b},t)]\rangle, \tag{8b}$$

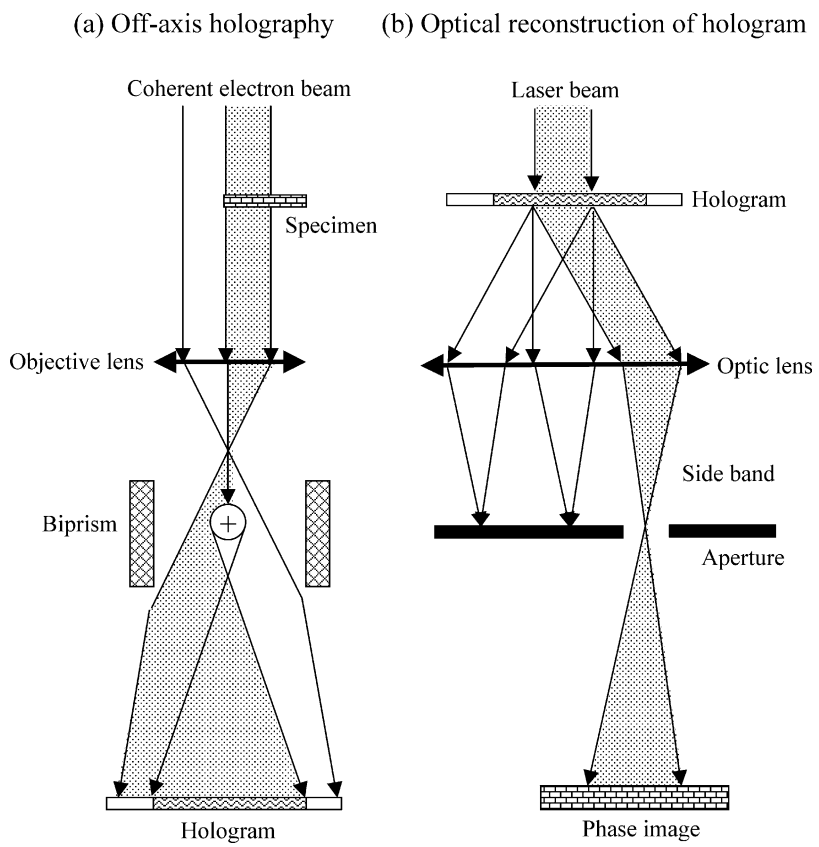

Fig. 4. (a) Formation of off-axis electron hologram in TEM using an electrostatic biprism, and (b) reconstruction of electron hologram using laser diffraction.

and

$$\langle \Delta A(\mathbf{b},t)\exp[\mathrm{i}\phi'(\mathbf{b},t)]\rangle = 0. \tag{8c}$$

Using the notations defined in Eqs. (8a)–(8c), Eq. (7) becomes

$$\begin{aligned}\mathrm{FT}[I_{\mathrm{hol}}(\mathbf{b})] =& \delta(\mathbf{u}) + \mathrm{FT}[A_0^2(\mathbf{b})] + \mathrm{FT}[\langle \Delta A^2(\mathbf{b},t)\rangle] \\ &+ \mathrm{FT}[A_0(\mathbf{b})\exp(\mathrm{i}\phi_0(\mathbf{b}))] * \delta(\mathbf{u}+\Delta\mathbf{K}) \\ &+ \mathrm{FT}[A_0(\mathbf{b})\exp(-\mathrm{i}\phi_0(\mathbf{b}))] * \delta(\mathbf{u}-\Delta\mathbf{K}).\end{aligned} \tag{9}$$

If the carrier spatial frequency $\Delta\mathbf{K}$ is sufficiently large, the sidebands do not overlap with the center band. By selecting only one sideband, say the band centered at $\mathbf{u} = -\Delta\mathbf{K}$, the electron wave function at the exit face of the specimen can be recovered to be $\langle \Psi(x,y,t)\rangle$. The reconstructed wave is a time averaged complex object wave, and can therefore be compared directly with the calculated electron wave function.

It is clear that TDS electrons (i.e. the $FT[\langle \Delta A^2(\mathbf{b},t)\rangle]$ term in Eq. (9)) is distributed only in the center band. This indicates that the TDS electrons will not contribute to the finally reconstructed phase image because it comes from the sideband (Wang, 1993). The only effect of TDS is to introduce an absorption function in the reconstructed amplitude image due to the time average. Therefore, it is possible that electron holography is an ideal energy-filter that even rules out the contribution made by TDS electrons if the electron source is monochromatic.

An experimental approach has been designed to test this prediction (Van Dyck et al., 2000). By simultaneously recording the off-axis electron hologram and the on-axis focal series of high-resolution TEM images from the same specimen region and under identical experimental conditions, the wave functions carried by the hologram and the high-resolution TEM images can be reconstructed, respectively, following the standard procedures (Zandbergen and Van Dyck, 2000). Such an experiment has been carried out by Lehmann and Lichte (2002), who found that the lattice fringe contrast reconstructed from the sideband is substantially higher than the contrast from HRTEM, and they suggested that the discrepancy is due to inelastic scattering. This conclusion proves the theoretically predicted result.

7. How does phonon scattering affect atomic-resolution lattice imaging?

As the image resolution is approaching 1 Å, quantitative matching of experimental images with the theoretically calculated images is needed for quantitative structure determination. Most of the available image calculation packages were developed with consideration of the contribution made by elastically scattered electrons, and

we are always puzzled why the calculated image, with consideration of all the possible instabilities in the experiments, has a better contrast than the observed image? One of the unresolved question is how does the TDS electron affect the image.

Before answering this question, one must examine the importance of TDS in electron diffraction and imaging. Shown in Fig. 5 is a group of energy-filtered electron diffraction patterns at high scattering angles, where the Kikuchi lines are clearly present. The patterns were formed by the electrons with different energy-losses so that the contributions made by the different processes can be separated. A line scan is made across the diffraction pattern for quantitative comparison purpose. In the pattern formed

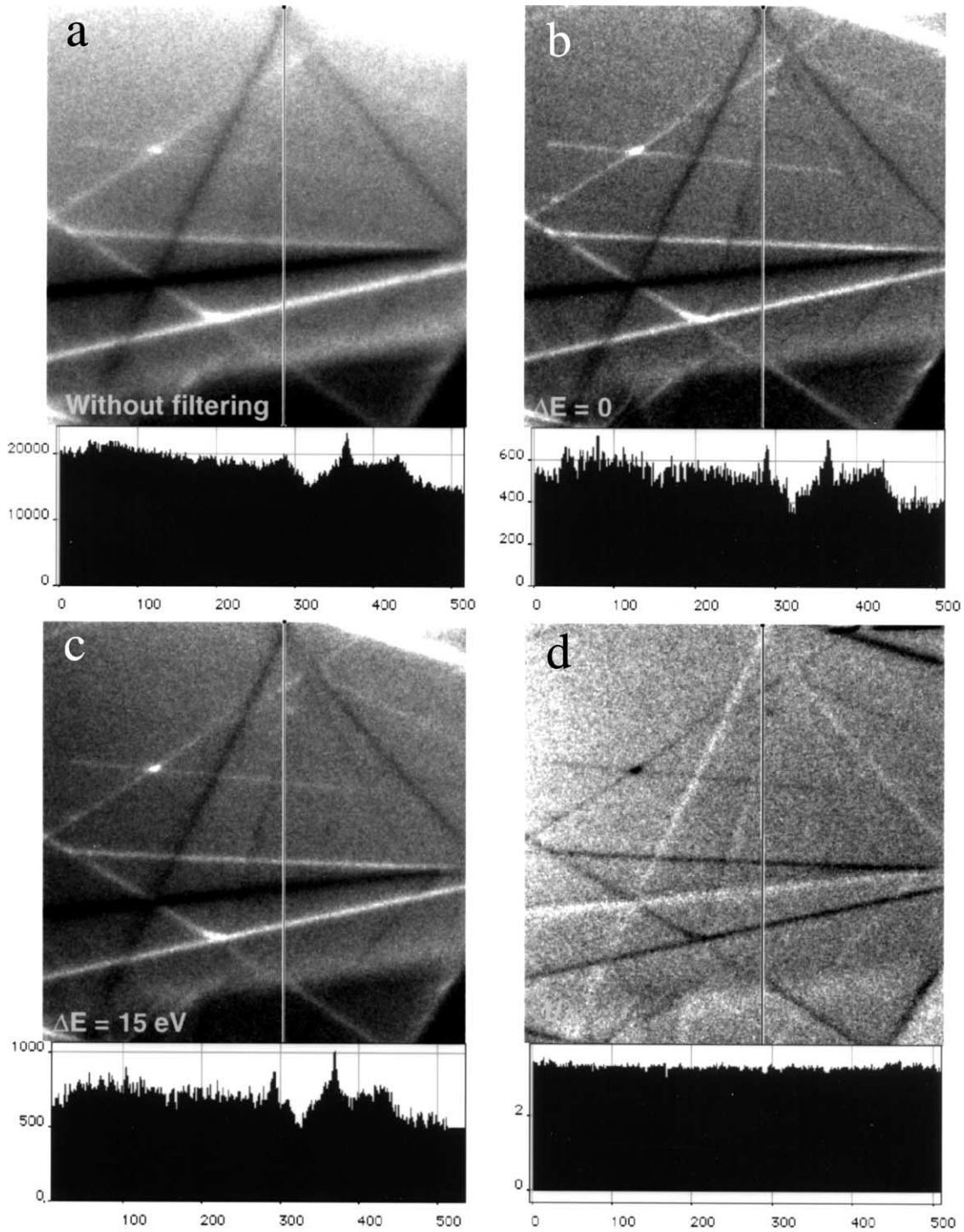

Fig. 5. Large angle Kikuchi patterns of Si recorded (a) without energy filtering, (b) using the electrons without energy-loss, and (c) with plasmon loss. (d) A thickness/mean-free-path image calculated from (a) and (b). The line scan profiles of the images are also shown to compare the absolute intensities.

by the electrons with energy losses smaller than the energy spread of the filament, typically 1.5 eV, the dominant contribution is TDS (Fig. 5b) because the elastic Bragg scattering does not fall into the angular range shown. The intensity taken by the first plasmon peak of GaAs is ~10% of the total intensity (Fig. 5c). The specimen thickness can be seen in the t/Λ image, where t is specimen thickness and Λ the electron mean free path length, which is ~80 nm for GaAs. For a specimen of thickness ~100 nm, the average intensity contributed by pure TDS electrons at high angles is ~27% of the total intensity excluding the component with larger energy-losses. These electrons come from the nuclear sites, and they can strongly affect the image contrast especially when the image resolution is high (Wang, 1999).

To simplify our discussion, the weak phase object approximation is used to illustrate the contribution made by TDS electrons in HRTEM images. The electron wave after exiting the crystal surface can be represented by

$$\Phi(\mathbf{b}) \approx 1 + \mathrm{i}\sigma V_{\mathrm{p}}(\mathbf{b}) = 1 + \mathrm{i}\sigma V_{\mathrm{p0}}(\mathbf{b}) + \mathrm{i}\sigma \Delta V_{\mathrm{p}}(\mathbf{b}, t), \quad (10)$$

where $\sigma = \pi/\lambda U_0, \mathbf{b} = (x, y)$, λ the electron wave length, U_0 the electron acceleration voltage, and V_{p} the instantaneous crystal projected potential. Taking a Fourier transform of the wave function

$$\Phi(\mathbf{u}) \approx \delta(\mathbf{u}) + \mathrm{i}\sigma \mathrm{FT}[V_{\mathrm{p0}}(\mathbf{b})] + \mathrm{i}\sigma \mathrm{FT}[\Delta V_{\mathrm{p}}(\mathbf{b}, t)], \quad (11)$$

where the first term is the center transmitted beam, the second term the Bragg reflected beams and the third term the diffusely scattered electrons. From the Abbe's imaging theory, the intensity seen in the image plane is

$$I(\mathbf{b}) = \langle |[1 + \mathrm{i}\sigma V_{\mathrm{p0}}(\mathbf{b}) + \mathrm{i}\sigma \Delta V_{\mathrm{p}}(\mathbf{b}, t)] * t_{\mathrm{obj}}(\mathbf{b})|^2 \rangle, \quad (12)$$

where $t_{\mathrm{obj}}(x, y)$ characterizes the information transfer of the objective lens and it is a Fourier transform of the objective lens transfer function $T_{\mathrm{obj}}(\mathbf{u})$, and $\langle\ \rangle$ represents the time average of the image intensity. With the use of $\langle \Delta V \rangle = 0$, the result is

$$I(\mathbf{b}) = 1 - 2\sigma V_{\mathrm{p0}}(\mathbf{b}) * \mathrm{Im}[t_{\mathrm{obj}}(\mathbf{b})] + \sigma^2 |V_{\mathrm{p0}}(\mathbf{b}) * t_{\mathrm{obj}}(\mathbf{b})|^2 + \sigma^2 \langle |\Delta V_{\mathrm{p}}(\mathbf{b}, t) * t_{\mathrm{obj}}(\mathbf{b})|^2 \rangle, \quad (13)$$

where the first term is the incident beam, the second term is the interference between the center beam with the Bragg diffracted beams (the first order effect), e.g. the bright-field lattice image, the third term is the interference between the Bragg reflected beams (the second order effect), and the last term is the contribution made by TDS (the second order effect). This equation clearly shows that the contribution made by TDS is on the same order of magnitude as the cross interference term between Bragg beams (Fig. 6a) excluding the central transmitted beam (Wang, 1998c), since ΔV is comparable to V_0 according to Fig. 2.

On the image contrast, the second term (the bright field term) can produce contrast reversal as the lens defocus is changed, but the intensity contributed by TDS is always the strongest at the atom sites. Therefore, at the Schertzer defocus condition under which the atomic columns show dark contrast, adding the TDS contribution reduces the darkness of the atom columns, resulting in a decrease in the image contrast (see Fig. 6b), possibly giving a better fit to the experimental image. This is the importance of TDS in HRTEM. This simple physical illustration can be spelled out using full quantum mechanical approach, leading to a new theory for calculating the images formed by phonon scattered electron in HRTEM with inclusion of full dynamic effects (Wang, 1998b). Most of the software packages currently available for image and diffraction pattern simulations, however, do not include the contribution made by TDS.

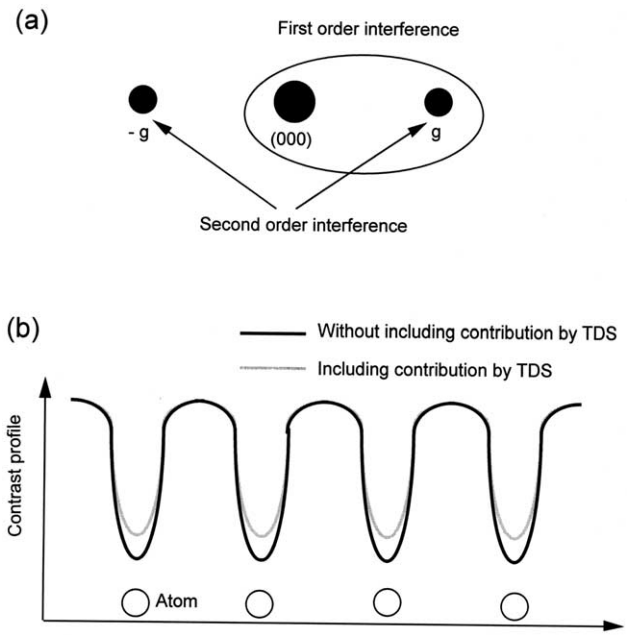

Fig. 6. (a) Lattice images can be formed by the interference of the central transmitted beam (000) and the diffracted beams. The cross-interference between the Bragg beams is the second order effect, which is equivalent to the contribution made by TDS in the imaging. (b) The reduction of the image contrast at the atom sites due to TDS under the Schertzer defocus.

8. Dynamic diffraction theory of diffusely scattered electrons

Conventional HRTEM is dominated by phase-contrast, which is the coherent interference property of elastically scattered waves. The HRTEM images are usually recorded without the use of an energy filter, so that both the elastically and inelastically scattered electrons contribute to the image. The inelastically scattered electrons tend to reduce the image contrast due to their incoherence and the effects of chromatic aberration. This makes quantitative data analysis difficult because only the elastic scattering of electrons can be accurately simulated using dynamic theories. For consideration of the excitation probabilities

of inelastic processes, TDS and plasmon excitation are the two main concerns. The image formed by the plasmon-loss electrons can be effectively represented by a defocus shift due to chromatic aberration (Wang and Bentley, 1991). These electrons can be filtered away experimentally, but the TDS electron remain. Our following analysis is concentrated on TDS electrons.

Diffuse scattering is produced by structure modulation in a crystalline specimen, and it is usually distributed between the Bragg reflected peaks. The Bragg reflections are generated by the periodically structured lattice of the crystal, while the diffuse scattering is produced by the non-periodical components including thermal vibrations of the crystal atoms and short-range order (SRO) of defects. TDS exists even for a perfect crystal without defects because atomic vibration is a non-periodic perturbation on the crystal potential. The typical character of diffuse scattering produced by SRO is that the patterns are complex, while the diffuse streaks in TDS case are usually along the interconnection lines among the Bragg reflections. This is likely due to the statistical correlated distribution of point defects. These patterns contain the spatial correlation function of the point defects, but their analysis is rather difficult because of the complication from dynamic diffraction effects.

8.1. The first order diffuse scattering theory

In this section, we present a general approach for dealing with diffuse scattering, produced by both phonons and point defects, in electron diffraction with consideration of full dynamic diffraction effects. There are three key challenges to the dynamic theory for diffusely scattered electrons. First, the theory should be able to include non-periodic structure in the calculation. Second, the contributions made by a variety of statistically distributed thermal vibration configurations of the lattice as well as the spatial variation in distribution of point defects must be summed incoherently, e.g. $I = \langle|\Psi|^2\rangle$. More importantly, a time and configuration average is required to be performed analytically before numerical calculation. Finally, the high order diffuse scattering may also need to be taken into account for thicker specimens.

The first order scattering theory demonstrated below are adequate for solving the first two challenges. For simplicity, we start from the time-independent Schrödinger equation by separating the crystal potential into a periodic component and a non-periodic one,

$$\left(-\frac{\hbar^2}{2\mathrm{m}_0}\nabla^2 - eV_0 - e\Delta V - E\right)\Psi = 0. \tag{14}$$

For diffraction calculation, the Green's function theory is the most convenient choice. Shifting the ΔV term to the right-hand side, Eq. (14) is converted into an integral equation with the use of the Green's function $G(r, r_1)$ (Kainuma et al. 1976):

$$\Psi(r,t) = \Psi_0(K_0, r) + \int \mathrm{d}\mathbf{r}_1 G(\mathbf{r}, \mathbf{r}_1)[e\Delta V(\mathbf{r}_1, t)\Psi(\mathbf{r}_1, t)], \tag{15}$$

where G is the solution of

$$\left(-\frac{\hbar^2}{2m_0}\nabla^2 - eV_0 - E\right)G(\mathbf{r}, \mathbf{r}_1) = \delta(\mathbf{r} - \mathbf{r}_1); \tag{16}$$

and $\Psi_0(\mathbf{K}_0, r)$ is the elastic wave scattered by the periodic, time-independent average potential V_0 due to an incident plane wave with wave vector $\mathbf{K}_0$ and it satisfies

$$\left(-\frac{\hbar^2}{2m_0}\nabla^2 - eV_0 - E\right)\Psi_0 = 0. \tag{17}$$

Eq. (17) can be solved using the Bloch wave or multislice theory (Van Dyck, 1985; Chen and Van Dyck, 1997). It must be pointed out that the time variable in Eq. (15) represents the instantaneous lattice configuration of the crystal due to thermal vibration. The diffraction pattern is calculated under the first order diffuse scattering approximation: $\Psi(r_1, t)$ is replaced by $\Psi_0(K_0, r_1)$ in Eq. (15), leading to

$$\Psi(\mathbf{r}, t) \approx \Psi_0(\mathbf{K}_0, \mathbf{r}) + \int \mathrm{d}\mathbf{r}_1 G(\mathbf{r}, \mathbf{r}_1)[e\Delta V(\mathbf{r}_1, t) \times \Psi_0(\mathbf{K}_0, \mathbf{r}_1)]. \tag{18}$$

This approximation holds if the diffuse scattering is much weaker than the Bragg reflections, and it is a good approximation for a general purpose (Fanidis et al., 1989). A detailed application of Eq. (18) to the diffraction of diffuselly scattered electrons arisen from TDS and SRO has been given elsewhere (Wang, 1996a).

8.2. High order diffuse scattering theory

Since our calculation is made based on the first order diffuse scattering approximation, the higher-order diffuse scattering terms are dropped. This approximation fails if the specimen is thick and/or the disorder is high. We now modify the solution Ψ_0 of Eq. (17) to compensate for these high order diffuse scattering terms so that the theory can be expanded to cases unrestricted by the first order diffuse scattering approximation. A correction potential$V^{(i)}$ is symbolically introduced,

$$\left(-\frac{\hbar^2}{2m_0}\nabla^2 - eV_0 - eV^{(i)} - E\right)\Psi_0 = 0. \tag{19}$$

The potential $V^{(i)}$ is chosen so that Eq. (28) exactly satisfies the original Schrödinger Eq. (14), which requires the potential $V^{(i)}$ to be

$$[V^{(i)}\Psi_0] = e\int \mathrm{d}\mathbf{r}_1[G(\mathbf{r}, \mathbf{r}_1)\Delta V(\mathbf{r}, \mathrm{t})\Delta V(\mathbf{r}_1, t) \times \Psi_0(\mathbf{K}_0, \mathbf{r}_1)]. \tag{20}$$

We now prove that the potential $V^{(i)}$ given by Eq. (20) can be applied to recover the high order diffuse scattering terms dropped when $\Psi(r_1,t)$ is replaced by $\Psi_0(K_0,r_1)$ in deriving Eq. (18) under the first order diffuse scattering approximation (Wang, 1996b). Starting from the integral form of Eq. (19) with the use of the Green's function and iterative calculation, the elastic wave is expanded as

$$\begin{aligned}\Psi_0(\mathbf{K}_0,\mathbf{r}) =& \Psi_0^{(0)}(\mathbf{K}_0,\mathbf{r}) + e\int d\mathbf{r}_1 G(\mathbf{r},\mathbf{r}_1)\\ &\times [V^{(i)}(\mathbf{r}_1\Psi_0(\mathbf{K}_0,\mathbf{r}_1)] = \Psi_0^{(0)}(\mathbf{K}_0,\mathbf{r})\\ &+ e^2\int d\mathbf{r}_1 G(\mathbf{r},\mathbf{r}_1)\int d\mathbf{r}_2[G(\mathbf{r}_1,\mathbf{r}_2)\Delta V(\mathbf{r}_1,t)\\ &\times \Delta V(\mathbf{r}_2,t)\Psi_0(\mathbf{K}_0,\mathbf{r}_2)] = \Psi_0^{(0)}(\mathbf{K}_0,\mathbf{r})\\ &+ e^2\int d\mathbf{r}_1\int d\mathbf{r}_2 G(\mathbf{r},\mathbf{r}_1)G(\mathbf{r}_1,\mathbf{r}_2)\Delta V(\mathbf{r}_1,t)\\ &\times \Delta V(\mathbf{r}_2,t)\Psi_0^{(0)}(\mathbf{K}_0,\mathbf{r}_2) + e^4\int d\mathbf{r}_1\int d\mathbf{r}_2\\ &\times\int d\mathbf{r}_3\int d\mathbf{r}_4 G(\mathbf{r},\mathbf{r}_1)G(\mathbf{r}_1,\mathbf{r}_2)\\ &\times G(\mathbf{r}_2,\mathbf{r}_3)G(\mathbf{r}_3,\mathbf{r}_4)\Delta V(\mathbf{r}_1,t)\Delta V(\mathbf{r}_2,t)\\ &\times \Delta V(\mathbf{r}_3,t)\Delta V(\mathbf{r}_4,t)\Psi_0^{(0)}(\mathbf{K}_0,\mathbf{r}_4)+\cdots \end{aligned} \tag{21}$$

where $\Psi_0^{(0)}$ is the Bragg scattered wave due to the average periodic lattice at the absence of $V^{(i)}$ (e.g. no absorption)

$$\left(-\frac{\hbar^2}{2m_0}\nabla^2 - eV_0 - E\right)\Psi_0^{(0)} = 0. \tag{22}$$

This equation can be solved using conventional dynamic electron diffraction theory (for a comprehensive review see Wang (1995)). Substituting Eq. (21) into Eq. (18), the total scattered wave is

$$\begin{aligned}\Psi(\mathbf{r},t) =& \Psi_0^{(0)}(\mathbf{K}_0,\mathbf{r}) + e\int d\mathbf{r}_1 G(\mathbf{r},\mathbf{r}_1)\Delta V(\mathbf{r}_1,t)\\ &\times \Psi_0^{(0)}(\mathbf{K}_0,\mathbf{r}_1) + e^2\int d\mathbf{r}_1\int d\mathbf{r}_2 G(\mathbf{r},\mathbf{r}_1)G(\mathbf{r}_1,\mathbf{r}_2)\\ &\times \Delta V(\mathbf{r}_1,t)\Delta V(\mathbf{r}_2,t)\Psi_0^{(0)}(\mathbf{K}_0,\mathbf{r}_2) + e^3\int d\mathbf{r}_1\int d\mathbf{r}_2\\ &\times\int d\mathbf{r}_3 G(\mathbf{r},\mathbf{r}_1)G(\mathbf{r}_1,\mathbf{r}_2)G(\mathbf{r}_2,\mathbf{r}_3)\Delta V(\mathbf{r}_1,t)\\ &\times \Delta V(\mathbf{r}_2,t)\Delta V(\mathbf{r}_3,t)\Psi_0^{(0)}(\mathbf{K}_0,\mathbf{r}_3)\\ &+ e^4\int d\mathbf{r}_1\int d\mathbf{r}_2\int d\mathbf{r}_3\int d\mathbf{r}_4 G(\mathbf{r},\mathbf{r}_1)G(\mathbf{r}_1,\mathbf{r}_2)\\ &\times G(\mathbf{r}_2,\mathbf{r}_3)G(\mathbf{r}_3,\mathbf{r}_4)\Delta V(\mathbf{r}_1,t)\Delta V(\mathbf{r}_2,t)\\ &\times \Delta V(\mathbf{r}_3,t)\Delta V(\mathbf{r}_4,t)\Psi_0^{(0)}(\mathbf{K}_0,\mathbf{r}_4)+\cdots \end{aligned} \tag{23}$$

This Born series is the exact solution of Eq. (14) without making any approximation. The third term in Eq. (23) is taken as an example to show its physical meaning. The Bragg scattered wave is diffusely scattered at r_2 by $\Delta V(r_2,t)$. The diffusely scattered wave is elastically scattered by the crystal lattice while propagating from r_2 to r_1 $[G(r_1,r_2)]$, then, the second order diffuse scattering occurs at r_1 $[\Delta V(r_1,t)]$. Finally, the double diffusely scattered wave exits the crystal at r after elastic scattering when propagating from r_1 to r $[G(r,r_1)]$. The integrals over r_1 and r_2 are to sum over the contributions made by all of the possible scattering sources in the crystal.

Therefore, the multiple diffusely scattered waves are comprehensively included in the calculation of Eq. (18) if the optical potential $V^{(i)}$ given by Eq. (20) is introduced in the calculation of Ψ_0 Eq. (1). This is a key conclusion which means that, by introducing a proper form of the optical potential, the multiple diffuse scattering terms are automatically included in the calculation using Eq. (18), although it was derived for the first order diffuse scattering. This result has a strong impact on the conventional diffuse scattering theories developed based on the first order diffuse scattering. Thus, an introduction of a complex potential $V^{(i)}$ in the calculation of the elastic wave makes the existing theories available for calculating the TDS and SRO including all orders of effects. This conclusion is universal for a time-independent system because no assumption and approximation was made in the proof.

We now examine the optic potential $V^{(i)}$, which is determined by

$$\begin{aligned}[V^{(i)}\Psi_0] =& e\int d\mathbf{r}_1[G(\mathbf{r},\mathbf{r}_1)\langle\Delta V(\mathbf{r},t)\Delta V(\mathbf{r}_1,t)\rangle\\ &\times \Psi_0(\mathbf{K}_0,\mathbf{r}_1)],\end{aligned} \tag{24}$$

To examine the meaning of Eq. (24), one ignores the diffraction effect of the crystal so that the Green's function is replaced by its free-space form:

$$G_0(\mathbf{r},\mathbf{r}_1) \approx \frac{2m_0}{\hbar^2}\frac{\exp(2\pi iK|\mathbf{r}-\mathbf{r}_1|)}{4\pi|\mathbf{r}-\mathbf{r}_1|}, \tag{25}$$

using the dynamic form factor defined in following

$$\begin{aligned}&\langle\Delta V(\mathbf{r}_1,t)\Delta V^*(\mathbf{r}_2,t)\rangle\\ &\quad= \int d\mathbf{Q}\int d\mathbf{Q}'\exp[2\pi i(\mathbf{r}_1\mathbf{Q}-\mathbf{r}_2\mathbf{Q}')]S(\mathbf{Q},\mathbf{Q}'),\end{aligned} \tag{26}$$

Eq. (24) is converted into

$$\begin{aligned}[V^{(i)}\Psi_0] \approx& \frac{m_0 e}{2\pi\hbar^2}\int d\mathbf{Q}\int d\mathbf{Q}' S(\mathbf{Q},\mathbf{Q}')\int d\mathbf{r}_1\\ &\times\left\{\frac{\exp(2\pi iK|\mathbf{r}-\mathbf{r}_1|)}{|\mathbf{r}-\mathbf{r}_1|}\exp[2\pi i(\mathbf{r}\mathbf{Q}-\mathbf{r}_1\mathbf{Q}')]\right.\\ &\left.\times\Psi_0(\mathbf{K}_0,\mathbf{r}_1)\right\},\end{aligned} \tag{27}$$

This potential is non-local function because $V^{(i)}$ cannot be separated from wave function Ψ_0. The most accurate representation of this non-local imaginary component is to use its Fourier coefficients given in a matrix form; the $(\mathbf{g},\mathbf{h})$

matrix elements are given by

$$V_{gh}^{(i)} \approx \frac{em_0}{2\pi^2\hbar^2 V_c}\left\{\int d\tau(\mathbf{u})\frac{S(\mathbf{k}_g-\mathbf{u},\mathbf{k}_h-\mathbf{u})}{u^2-K_0^2} + i\frac{\pi}{2K_0}\int d\sigma(\mathbf{u})S(\mathbf{k}_g-\mathbf{u},\mathbf{k}_h-\mathbf{u})\right\}, \quad (28)$$

where V_c is the volume of the crystal; the integral $\tau(u)$ is over all reciprocal space $\mathbf{u}$ except a spherical shell defined by $|\mathbf{u}| = K_0$; and the integral $\sigma(\mathbf{u})$ is on the surface of the Ewald sphere defined by $|\mathbf{u}| = K_0$, with $k_g \approx K_0 + g$ and $k_h \approx K_0 + h$. The dynamic form factor S is the most important function in this calculation. From Eq. (28), the correction potential $V^{(i)}$ is a complex function, its imaginary component denotes the 'absorption' effect. Therefore, the potential V introduced in Eq. (20) is the absorption potential defined by Yoshioka (1957) under the first order approximation, which represents the effect of the TDS on the elastic scattered wave. On the other hand, if the Green's function takes its real solution rather than the form in free-space (Eq. (26)), the high order expressions of this potential contain the high order diffuse scattering terms dropped under the first order diffuse scattering approximation. In other words, the higher order terms of $V^{(i)}$ represents the contribution of the TDS electron to the image/diffraction pattern. This is the part that, unfortunately, had been lost in the literature. An accurate calculation of this potential is given elsewhere (Wang, 1998c).

In summary, by inclusion of a complex potential in dynamic calculation, the high order diffuse scattering is fully recovered in the calculations using the equation derived under the distorted wave Born approximation, and more importantly, the statistical time and structure averages over the distorted crystal lattices are evaluated analytically prior to numerical calculation. This conclusion establishes the basis for expanding the applications of the existing theories. Therefore, the absorption potential has a much more rich meaning than the conventional interpretation of an absorption effect.

Theoretical calculation of the absorption potential is a rather sophisticated process. Band structure calculation is required for dealing with plasmon excitation, and the result could be surprising in a way that plasmon scattering could be more localized than expected (Forsyth et al., 1997). Calculations of Eq. (29) for TDS and inner shell ionization have been performed (Allen and Rossouw, 1990). Anisotropic thermal vibration can make appreciable contribution to the calculated absorption potential (Peng, 1997).

8.3. What is missing in conventional image calculation?

Most of the dynamic calculations reported in the literature are performed with including the Debye–Waller factor and an imaginary absorption potential following an equation of

$$\left(-\frac{\hbar^2}{2m_0}\nabla^2 - eV_0 - eV^{(i)} - E\right)\Psi_0 = 0. \quad (29)$$

We would like to know what is missing in this type of traditional calculation. To illustrate this point one starts from the Born series solution of Eq. (29), which is

$$\begin{aligned}\Psi_0(\mathbf{K}_0,\mathbf{r}) &= \Psi_0^{(0)}(\mathbf{K}_0,\mathbf{r}) + e\int d\mathbf{r}_1 G(\mathbf{r},\mathbf{r}_1)[V^{(i)}(\mathbf{r}_1)\Psi_0(\mathbf{K}_0,\mathbf{r}_1)]\\ &= \Psi_0^{(0)}(\mathbf{K}_0,\mathbf{r}) + e^2\int d\mathbf{r}_1\{G(\mathbf{r},\mathbf{r}_1)\int d\mathbf{r}_2[G(\mathbf{r}_1,\mathbf{r}_2)\\ &\quad\times\Delta V(\mathbf{r}_1,t)\Delta V(\mathbf{r}_2,t)\Psi_0(\mathbf{K}_0,\mathbf{r}_2)]\}\\ &= \Psi_0^{(0)}(\mathbf{K}_0,\mathbf{r}) + e^2\int d\mathbf{r}_1\int d\mathbf{r}_2[G(\mathbf{r},\mathbf{r}_1)G(\mathbf{r}_1,\mathbf{r}_2)\\ &\quad\times\Delta V(\mathbf{r}_1,t)\Delta V(\mathbf{r}_2,t)\Psi_0^{(0)}(\mathbf{K}_0,\mathbf{r}_2)] + e^4\int d\mathbf{r}_1\\ &\quad\times\int d\mathbf{r}_2\int d\mathbf{r}_3\int d\mathbf{r}_4[G(\mathbf{r},\mathbf{r}_1)G(\mathbf{r}_1,\mathbf{r}_2)G(\mathbf{r}_2,\mathbf{r}_3)\\ &\quad\times G(\mathbf{r}_3,\mathbf{r}_4)\Delta V(\mathbf{r}_1,t)\Delta V(\mathbf{r}_2,t)\Delta V(\mathbf{r}_3,t)\\ &\quad\times\Delta V(\mathbf{r}_4,t)\Psi_0^{(0)}(\mathbf{K}_0,\mathbf{r}_4)] + \cdots \end{aligned} \quad (30)$$

In comparison with Eq. (23), the odd power terms of ΔV are missing. Therefore, in the classical dynamic calculation using either the Bloch wave or multislice theory, the contribution made by the second, fourth and all the even power order diffuse scattering terms are included, but the first, third and all the even order diffuse scattering terms are ignored. Thus, the calculation includes only a small portion of the diffuse scattering (e.g. the absorption effect from diffuse scattering), and the calculated results should be considered as pure-elastic Bragg scattering only.

The approximations made in conventional calculations are summarized in the following. First, the Green function G is replaced by its form in free-space G_0, which means that the dynamic elastic diffraction of the electrons is ignored once they are diffusely scattered (Fig. 7). Second, the optical potential $V^{(i)}$ is usually approximated as an imaginary function and the real part is ignored. This might be a good approximation for TDS, but it may not hold for SRO of point defects. Third, the first, third and all odd power terms of the diffuse scattering terms are dropped. Since the diffuse scattering is mainly distributed at high scattering angles for TDS, in the low scattering angular range the calculation accounts only for the purely Bragg reflections although the Debye–Waller factor is included; in the high angle range, the calculation accounts only for a small portion of the diffuse scattering. Finally, it must be pointed out that the Debye–Waller factor characterizes the weakening of atomic scattering factor due to the blurring effect of the atom thermal vibration, but the inclusion of this factor does not mean that the diffuse scattering is included in the calculation. This has been misunderstood by many readers.

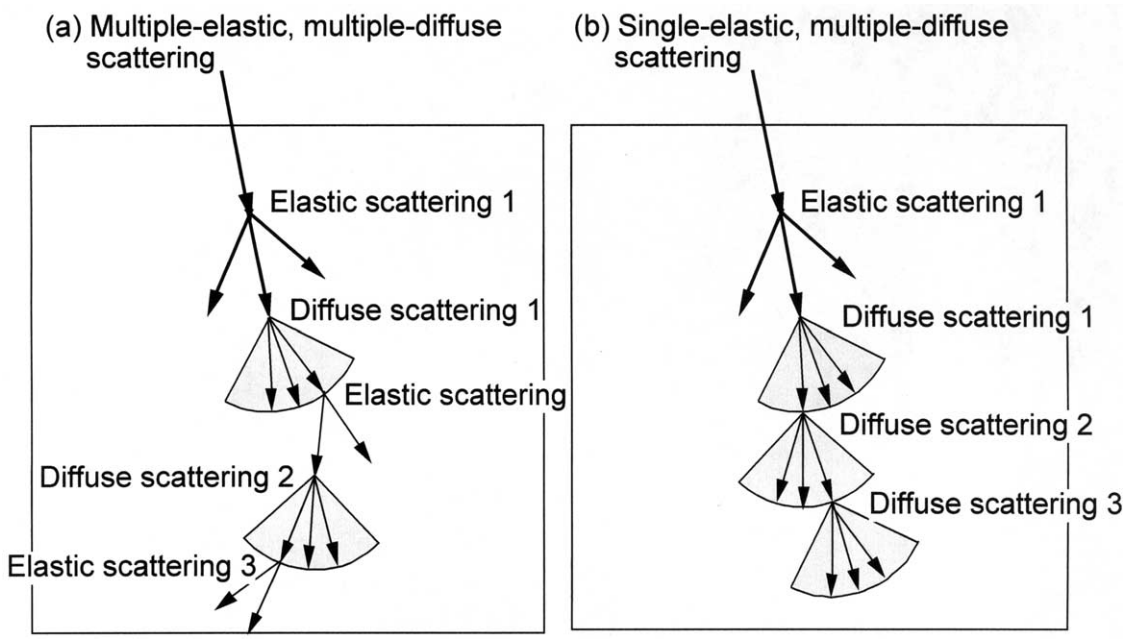

Fig. 7. Schematic diagrams showing multiple diffuse scattering processes in a crystal (a) with (G) and (b) without (G_0) consideration of dynamic diffraction between consecutive diffuse scattering events. The fan-shape represents the intensity angular distribution due to a diffuse scattering event.

9. Summary

With the help of an energy-filter, most of the inelastic signals can be removed from the image except phonon scattered electrons. This paper reviews a few studies that we have carried out in quantifying the contribution made by TDS electrons in quantitative electron microscopy, in following topics.

1. The contribution from TDS electrons is especially important if the image resolution is approaching 0.1 nm and beyond with the introduction of Cs corrected microscopes. It is shown that the contribution of the TDS electrons to the image is of the same order as the cross interference terms for the Bragg reflected beams in the dark-field high-resolution TEM imaging. In quantitative HRTEM, the theoretically calculated images usually give better contrast than the experimentally observed ones although all of the factors have been accounted for. This discrepancy is suggested due to TDS. A more rigorous multislice theory has been developed to account for this effect (Wang, 1998c).
2. Back to 1993 (Wang, 1993), we proposed theoretically that the off-axis holography is an ideal energy filter that even filters away the contribution made by TDS electrons in the electron wave function, but conventional high-resolution microscopy do contain the contribution made by phonon scattered electrons. The only effect of TDS is to introduce an absorption function in the reconstructed amplitude image due to the time average, but no effect on the phase image. This theoretical hypothesis now has been proved experimentally.
3. In electron scattering, most of the existing dynamical theories have been developed under the first order diffuse scattering approximation; thus, they are restricted to cases where the lattice distortion is small. A formal dynamical theory is presented for calculating diffuse scattering with the inclusion of multiple diffuse scattering (Wang, 1996b). By inclusion of a complex potential in dynamical calculation, a rigorous proof is given to show that the high order diffuse scattering are fully recovered in the calculations using the equation derived under the distorted wave Born approximation, and more importantly, the statistical time and structure averages over the distorted crystal lattices are evaluated analytically prior numerical calculation. This conclusion establishes the basis for expanding the applications of the existing theories.
4. The meaning of the absorption potential introduced in conventional calculation was explored extensively. In addition to illustrating its role in representing the absorption effect, emphasis was on its relationship with high order diffuse scattering. This is a remarkable advance in electron diffraction theory because it had been a problem in dealing with the dynamic diffraction of diffusely scattered electrons from both TDS and SRO of point defects. The importance of TDS in quantitative high-resolution TEM was also addressed.
5. The frozen lattice model is a semi-classical approach for calculating electron diffuse scattering in crystals arisen from thermal vibration of crystal atoms. This

quasi-elastic scattering approach is, however, concerned since its equivalence with the incoherent phonon excitation model is not yet established. Based on a rigorous quantum mechanical phonon excitation theory, we have proved that an identical result would be obtained using the frozen lattice model and the formal phonon excitation model if, (1) the incoherence between different orders of thermal diffuse scattering is considered in the frozen lattice model calculation, and (2) the specimen thickness and the mean-free-path length for phonon excitation both are smaller than the distance traveled by the electron within the life-time of the phonon ($\sim 5\,\mu m$ for 100 kV electrons). Condition (2) is usually absolutely satisfied and condition (1) can be precisely accounted for in the calculation with the introduction of the mixed dynamic form factor $S(\mathbf{Q}, \mathbf{Q}')$. The conclusion holds for each and all of the orders of diffuse scattering, thus, the quantum mechanical basis of the frozen lattice model is established, confirming the validity, reliability and accuracy of using the frozen lattice model in quantitative dynamical electron diffraction and imaging calculations.

References

Allen, L.J., Rossouw, C.J., 1990. Absorption potentials due to ionization and thermal diffuse scattering by fast electrons in crystals. Phys. Rev. B 42, 11644–11654.

Batson, P.E., Nellby, N., Krivanek, 2002. Sub-angstron resolution using aberration corrected electron optics. Nature 418, 617–620.

Chen, J.H., Van Dyck, D., 1997. Accurate multislice theory for elastic electron scattering in transmission electron microscopy. Ultramicroscopy 70, 29–44.

Crewe, A.V., 1978. Direct imaging of single atoms and molecules using the STEM. Chem. Scripta. 14, 17–20.

Fanidis, C., Van Dyck, D., Coene, W., Van Landuyt, J., 1989. Thermal atom motion in the simulation of high resolution images and electron diffraction patterns. In: Krakow, W., O'Keefe, M. (Eds.), Computer Simulation of Electron Microscope Diffraction and Images, The Minerals, Metals and Materials Society, pp. 135–158.

Fanidis, C., Van Dyck, D., Van Landuyt, J., 1992. Inelastic scattering of high-energy electrons in a crystal in thermal equilibrium with the environment, I. Theoretical framework. Ultramicroscoopy 41, 55–64.

Fanidis, C., Van Dyck, D., Van Landuyt, J., 1993. Inelastic scattering of high-energy electrons in a crystal in thermal equilibrium with the environment, II. Solution of the equations and applicatioins to concrete cases. Ultramicroscoopy 41, 55–64.

Forsyth, A.J., Smith, A.E., Josefsson, T.W., 1997. Virtual scattering of high-energy electrons by plasmons and valence electrons in silicon. Acta Crystallogr. A 53, 523–525.

Garmestani, H., Kalu, P., Dingley, D., 1998. Characterization of Al-8090 superplastic materials using orientation imaging microscopy. Mater. Sci. Engng A 242, 284–291.

Geipel, T., Mader, W., 1996. Practical aspects of hollow-cone imaging. Ultramicroscopy 63, 65–74.

Goldstein, J.I., Newbury, D.E., Echlin, P., Joy, D.C., Romig, A.D., Lyman, C.E., Fiori, C., Lifshin, E., 1992. Scanning Electron Microscopy and X-ray Microanalysis, a Text for Biologists, Materials Scientists and Geologists, Plenum Press, New York.

Goyal, A., Specht, E.D., Wang, Z.L., Kroeger, D.M., 1997. Grain boundary studies of high-temperature superconducting materials using electron backscatter Kikuchi diffraction. Ultramicroscopy 67, 35–57.

Hirsch, P.B., Howie, A., Nicholson, R., Pashley, D.W., Whelan, M.J., 1977. Electron microscopy of thin crystals, Krieger Publishing Co, New York.

Kainuma, Y., Kashiwase, Y., Kogiso, M., 1976. Thermal diffuse scattering in electron diffraction. J. Phys. Soc. Jpn 40, 1707–1712.

Fu, Q., Lichte, H., Volkl, E., 1991. Correction of aberrations of an electron-microscope by means of electron holography. Phys. Rev. Lett. 67, 2319–2322.

Lehmann, M., Lichte, H., 2002. Contribution of elastically and inelastically scattered electrons to high-resolutioin off-axis electron holograms—a quantitative analysis. Microsc. Microanal. 8 (Suppl. 8), 34–35.

Loane, R.F., Xu, P., Silcox, J., 1991. Thermal vibratioins in convergent-beam electron diffraction. Acta Crystallogr. A 47, 267–278.

Muller, D.A., Edwards, B., Kirkland, E.J., Silcox, J., 1997. Detailed calculations of thermal diffuse scattering. Microsc. Microanal. 3 (Suppl. 2), 1153–1154.

Omoto, K., Tsuda, K., Tanaka, M., 2002. Simulations of Kikuchi patterns due to thermal diffuse scattering on MgO crystals. J. Electron Microsc. 51, 67–78.

Peng, L.M., 1997. Anisotropic thermal vibrations and dynamical electron diffraction by crystals. Acta Crystallogr. A 53, 663–672.

Peng, L.M., Ren, G., Dudarev, S.L., Whelan, M.J., 1996. Debye–Waller factors and absorptive scattering factors of elemental crystals. Acta Crystallogr. A 52, 456–470.

Pennycook, S.J., Jesson, D.E., 1990. High-resolution incoherent imaging of crystals. Phys. Rev. Lett. 64, 938–941.

Sears, V.F., Shelley, S.A., 1991. Debye–Waller factor for elemental crystals. Acta Crystallogr. A 47, 441–446.

Sidorov, M.V., McCartney, M.R., Smith, D.J., 1997. High resolution TEM imaging with hollow-cone illumination. Microsc. Microanal. 3 (Suppl. 2), 1191–1192.

Takagi, S., 1958. On the temperature diffuse scattering of electrons I. Derivation of general formulae. J. Phys. Soc. Jpn 13, 278–286.

Tonomura, A., 1993. Electron Holography, Springer, New York.

Van Dyck, D., 1985. Image calculations in high-resolutioin electron microscopy problems, progress and prospects. Adv. Electr. Electron Phys. 65, 295–355.

Van Dyck, D., Lichte, H., Spence, J.C.H., 2000. Inelastic scattering and holography. Ultramicroscopy 81, 187–194.

Wang, Z.L., 1993. Thermal diffuse scattering in high-resolution electron holography. Ultramicroscopy 52, 504–511.

Wang, Z.L., 1994. Dislocation contrast in high-angle hollow-cone dark-field TEM. Ultramicroscopy 53, 73–90.

Wang, Z.L., 1995a. Elastic and Inelastic Scattering in Electron Diffraction and Imaging, Plenum Press, New York.

Wang, Z.L., 1995b. Dynamical theories of dark-field imaging using diffusely scattered electrons in STEM and TEM. Acta Crystallogr. A 51, 569–585.

Wang, Z.L., 1996a. Electron statistical dynamical diffuse scattering in crystals containing short-range order point defects. Acta Crystallogr. A 52, 717–729.

Wang, Z.L., 1996b. Statistical multiple diffuse scattering in a distorted crystal system—an exact theory. Phil. Mag. B 74, 733–749.

Wang, Z.L., 1998a. The frozen lattice A roach for incoherent phonon excitations in electron scattering, how accurate is it? Acta Crystallogr. A 54, 468–480.

Wang, Z.L., 1998b. An optical potential a roach to incoherent multiple thermal diffuse scattering in quantitative HRTEM. Ultramicroscopy 74, 7–26.

Wang, Z.L., 1998c. Green's function for electron scattering and its applications in low voltage point-projection microscopy and optical potential. Phil. Mag. B 77, 787–803.

Wang, Z.L., 1999. Phonon scattering, how does it affect the image contrast in high-resolution TEM? Phil. Mag. B 79, 37–48.
Wang, Z.L., Bentley, J., 1991. Microsc. Microstruct. Microanal. 2, 569.
Wang, Z.L., Cowley, J.M., 1989. Simulating high-angle annular dark field (ADF) STEM images including inelastic thermal diffuse scattering. Ultramicroscopy 31, 437–454.
Wang, Z.L., Cowley, J.M., 1990. Theory of high-angle annular dark field STEM images of Ge/Si interfaces. Ultramicroscopy 32, 275–289.
Yoshioka, H., 1957. Effect of inelastic waves on electron diffraction. J. Phys. Soc. Jpn 12, 618–628.
Zandbergen, H.W., Van Dyck, D., 2000. Exit wave reconstructions using through focus series of HREM images. Microsc. Res. Techniq. 49, 301–323.